Techno-Economic Analysis of WAMS Based Islanding Detection Algorithm for Microgrids with Minimal PMU in Smart Grid Environment

R. Rohikaa Micky, R. Sunitha, and S. Ashok

Abstract With large scale deployment of non dispatchable renewable energy sources, distributed generators (DGs) have paved way for multiple microgrids. Existing standards stipulate disconnection of DGs in the event of any fault in either utility or microgrid side. However, to ensure reliable power supply from these microgrids, the proposed scheme operates an islanding detection algorithm (IDA) employed at the microgrid control center (MGCC) that acts on the switch at the utility point of common coupling (PCC). The whole microgrid is switched over to an islanded mode on detection of an islanding event. Phasor measurement unit (PMU) data from the utility PCC enables accurate islanding detection using islanding detection monitoring factor (IDMF) and rate of change of inverse hyperbolic cosecant function of voltage (ROCIHCF) along with voltage at the PCC. Mathematical morphological filters are employed to detect any persistent short circuit fault in the microgrid side which may island the DG. For such faults, decision for disconnecting the DG or islanded operation is based on probability of power balance (PoB) and probability of islanding duration in the sub-microgrids, computed at the MGCC. Further, performance of the IDA in microgrids is assessed using a proposed, microgrid performance index (MGPI) considering the uncertainties in NDRES. Suitability of the proposed indices to predict events leading to islanded operation in real time is also validated using decision tree (DT) method. The discrimination capability between islanding and other transient events of DTs, yielded an accuracy of approximately 99.9% for minimum detection time, which proves the prowess of the method in real time scenario. Compared to existing methods, the proposed method promises reduced islanding detection time. Another distinct feature is that time for islanding detection remains same irrespective of power mismatch ratios. The proposed method

R. Rohikaa Micky (✉) · R. Sunitha · S. Ashok
Electrical Engineering Department, National Institute of Technology Calicut, Calicut, Kerala, India
e-mail: rohikaaeee@gmail.com

R. Sunitha
e-mail: rsunitha@nitc.ac.in

S. Ashok
e-mail: ashoks@nitc.ac.in

prevents false alarms for critical non-islanding events with zero non detection zone. Utilizing the proposed method, any redundant DG outage can be avoided, minimizing their down time. An economic analysis of the proposed islanding detection method using wide area monitoring system (WAMS) with minimal PMU deployment has also been studied to reduce the cost of PMU installation without sacrificing the reliability benefit for the customers.

Keywords Islanding detection · Smart grids · Microgrids · PMU · Islanding detection monitoring factor · Microgrid performance index · Smart grid

1 Introduction and Chapter Overview

Owing to rapid development of microgrids promoting non-dispatchable renewable energy sources (NDRES) worldwide due to the envisioned economic and environmental benefits, problems like voltage variations, reverse power flow, power fluctuations and power quality issues are encountered in the power system. Another such problem which arises with huge deployment of NDRES is occurrence of islanding events which if unnoticed is hazardous to service personnel, cause voltage and frequency changes and synchronization issues while reconnecting to utility grid (UG). In islanding condition, though the microgrid (MG) is electrically disconnected from the UG, the DG units remain still energized to meet the local load [1].

As per [2] DG should be discontinued from service in 2 s at the initiation of an islanding event (IE). However, this current practice is not a viable option as it disrupts reliable power supply to customers [3]. Instead, it would be pragmatic to permit islanded operation which ensure continuous supply to consumers. However, for this, safety of MG has to be studied at UG and microgrid levels. For fault in the UG, MG may be switched over to an isolated operation. An islanding detection algorithm (IDA) should have the ability to distinguish between UG and local microgrid faults [4]. During microgrid faults, islanding detection technique (IDT) needs to island only the smallest part of the faulted area as far as possible [5].

IDTs are broadly categorized into local and remote techniques. The former includes passive and active techniques. Passive IDTs do not function when there is zero power exchange between the utility and microgrid. Recent researches on passive IDT aimed to reduce non detection zone (NDZ) by utilizing rate of change of sequence components of currents [6] and mathematical morphology filters [7]. However, main shortcomings of these works are non- zero NDZ and spurious tripping during three phase faults involving ground. Also, many have not been tested for all the events occurring in the power system. Active IDTs have negligible NDZ, but it degrades power quality. Remote IDTs have null NDZ and depends on communication of data between the DGs and UG through power line carrier communication (PLCC), transfer trip and supervisory control and data acquisition (SCADA) schemes. Hybrid IDTs combine superior qualities of passive and active IDTs to reduce NDZ and power quality issues.

In the IDTs discussed previously, each distributed generator (DG) is lodged with an IDA. For faults in the MG, if healthy DGs are permitted to cater to the isolated network, blackouts may be prevented. However, control schemes in the isolated MG should be equipped with proper power sharing, frequency and voltage control algorithms. Majority of the existing techniques are based on faults in the UG side. In [8] only grid side fault is examined. Islanding was executed by opening UG circuit breaker in [9]. But, load was shed unnecessarily for minimising NDZ for low power mismatches and also the DG is disconnected for feeder loss within the MG.

Reference [10] suggests utilising a control centre while considering the whole MG as a "single DG block". Thus, efficient communication and intelligence protocols are required as an interface between UG, the islanded network and the microgrid control centre (MGCC). In this regard, [11] defined PCC as the point of coupling between utility and MG and the point of connection of utility with distributed energy resource (DER) as PoC. Therefore, it is essential to recognise every single IE so that MG may execute the isolated operation by coordinated action of inverter control and storage devices. Some of the few works which investigated possible islanded operation due to an IDT functioning from utility PCC can be found in [12, 13]. But these IDTs lacked proper definition of chosen threshold values and did not consider DG islanding situations arising due to feeder loss or faults remaining uncleared in the MG. Thus it is imperative to explore reliability of a robust IDA acting at the utility grid PCC and its potential to remove false alarms for events occurring in the UG or MG. Therefore, the work presented in this chapter proposes an IDA using passive technique and minimal number of phasor measurement units (PMUs) with reliable communication infrastructure which is presumed to be existing in the smart grid.

The remaining sections of the chapter are organised as follows. Section 2 presents an overview of the concept behind the proposed islanding detection algorithm. Implementation of the algorithm with the developed indices are discussed in Sect. 3. Result analysis for various islanding scenarios are demonstrated in Sect. 4 and in Sect. 5, an economic analysis has been performed for the proposed islanding detection with minimal PMU deployment. Real time islanding detection is carried out using decision tree technique in Sect. 6 and finally, conclusions are drawn in Sect. 7.

2 Concept of Proposed Islanding Detection Algorithm

Block diagram representation of the proposed IDA is depicted in Fig. 1. Power system parameters like voltage and current magnitudes, real, reactive and apparent powers are collected at the MGCC from PMUs. Further in MGCC, two proposed indices are calculated and the islanding detection algorithm is executed. Probability of power balance which indicates towards possible islanded operation is also estimated in the control centre. Based on the probability of power balance, microgrid performance index is obtained and this is further used for analysis of benefits accrued with regard to reduction in customer outage costs. Decision tree models are developed using
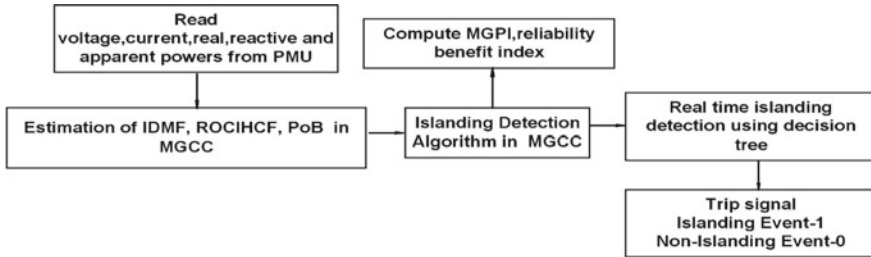
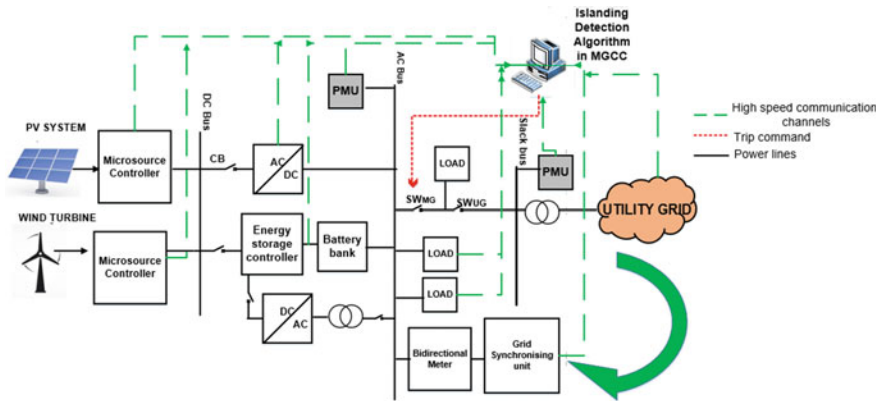**Fig. 1** Basic block diagram of the proposed IDA

Fig. 2 Schematic representation of proposed IDA

training and test data obtained from the proposed IDA from several scenarios in the system for real time islanding detection.

Figure 2 illustrates a typical MG consisting of one wind turbine, one PV panel, local loads, converters, and controllers for the sources and the load. Here, two phasor measurement units are deployed in the system one at the reference bus of the UG and other at the PCC of the whole microgrid. Time synchronized measurements are transferred to the MGCC where decisions are taken based on the IDA. In this work, IEs are analyzed for a whole MG which has multiple sub-microgrids within it. IDA in the MGCC sends signal to MG switch (SW$_{MG}$), so that the whole microgrid can be managed as an autonomous unit for disconnection of UG switch (SW$_{UG}$) and during any persistent fault in the utility side. In islanded mode, control techniques suggested in [14] can be utilized to maintain frequency and voltage within the constraints. Switches, SW$_{MG}$ and SW$_{UG}$ also prevent reconnection of the unsynchronized MG with the UG. Upon detection of a loss of feeder connected to DG either the control mode has to be switched to isolated mode or the DG needs to be decoupled. It is decided depending on probability of power balance (PoB) in the sub-microgrids. Voltage and current relays at the PoC send status of DGs to the MGCC. PoB of the

sub-microgrids is determined at the MGCC to command them for islanded operation. Authentic communication for two-way data exchange between utility, MGCC and PMUs is supposed to be existing in the smart grid as depicted in Fig. 2. Synchrophasor units transfer time synchronized current and voltage measurements from PCC to control centre through wide area communication technologies such as WiMAX, cellular, digital subscriber line and fibre optic networks.

Thus main features of the IDA are (1) islanding detection time is reduced as measurements are taken at the PCC of SW_{UG} instead of PoC of DG and the UG. (2) down time of sub islands can be minimised based on PoB. (3) On detection of loss of connection with the UG, the IDA switches open SW_{MG} at the PCC for islanded operation of MG. Another distinct feature of the proposed IDA is that only the fault affected DGs need to be disconnected when islanded operation is not feasible in the identified sub-microgrids. If PoB in the sub-microgrids is within the thresholds, the concerned DG along with its loads and energy units can be managed with proper reactive power/voltage control or real power/frequency control techniques in the sub-microgrids.

3 Implementation of the IDA

Here, effectiveness of the proposed IDA is demonstrated using 3 cases that might lead to islanding condition in a grid connected MG.

Case 1: IDA detects any inception of opening of utility side CB, isolators or switches. For fault in the MG, each DG is observed separately to prevent spurious tripping. PoB is monitored at each DG terminal. Cases II and III are considered which if undetected might threaten the microgrid security and reliability.

Case 2: Loss of feeders connecting DGs which might lead to DGs being disconnected from the utility.

Case 3: Permanent feeder fault in sub-microgrids which might lead to CB operation resulting in DG islanding. Control algorithm in DG switches over to autonomous mode if probability of power balance satisfies the threshold range in Cases II and III.

3.1 Case 1

The proposed IDA utilises two proposed indices along with voltage at the utility PCC. The indices along with their threshold and the algorithm is explained here. On islanding detection, control schemes may be adopted for islanded operation as in [14, 15].

Fig. 3 Thevenin equivalent
model of grid connected
microgrid
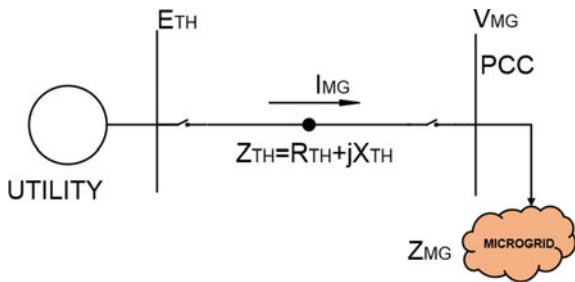
A. *Islanding Detection Monitoring Factor*

The whole grid with the DGs is modelled as an equivalent Thevenin network as in
Fig. 3. If utility grid voltage and microgrid impedance are E_{TH} and Z_{MG} respectively.
Then,

$$E_{TH} = V_{MG} + Z_{TH} I_{MG} \tag{1}$$

Here, V_{MG} and I_{MG} denote voltage and current at utility PCC of the MG. These
are measurable variables from phasor measurement units. E_{TH} and Z_{TH} denote utility
grid Thevenin voltage and impedance. (1) can be written in terms of Z_{TH} as:

$$E_{THr} + jE_{THIm} = (V_{MGr} + jV_{MGIm}) + (R_{TH} + jX_{TH})(I_{MG} + jI_{MGIm}) \tag{2}$$

E_{THr} and E_{THIm} denote real and imaginary parts of E_{TH}, V_{MGr} and V_{MGIm} represent
real and imaginary parts of V_{MG}. R_{TH}, X_{TH} are resistive and reactive parts of Z_{TH}
and I_{MGr}, I_{MGIm} are real and imaginary parts of current drawn by microgrid.

For a time *t,* four unknown variables namely, E_{THr}, E_{TIm}, R_{TH} and X_{TH} are solved
using V_{MG} and I_{MG} and by representing (2) in matrix form as (3) [16],

$$
\begin{bmatrix}
1 & 0 & -I_{MGr,1} & I_{MGIm,1} \\
0 & 1 & -I_{MGIm,1} & -I_{MGr,1} \\
1 & 0 & -I_{MGr,2} & I_{MGIm,2} \\
0 & 1 & -I_{MGIm,2} & -I_{MGr,2}
\end{bmatrix}
\begin{bmatrix}
E_{THr} \\
E_{THIm} \\
R_{TH} \\
X_{TH}
\end{bmatrix}
=
\begin{bmatrix}
V_{MGr,1} \\
V_{MGIm,1} \\
V_{MGr,2} \\
V_{MGIm,2}
\end{bmatrix}
\tag{3}
$$

Apparent power, S_{MG} drawn by MG isiven by (4) and (5).

$$S_{MG} = 3Z_{MG} I_{MG}^2 \tag{4}$$

If $\bar{Z_{MG}} = Z_{MG} \angle \alpha$ and $\bar{Z_{TH}} = Z_{TH} \angle \beta$

$$S_{MG} = \frac{E_{TH}^2 Z_{MG}}{Z_{TH}^2 + Z_{MG}^2 + 2Z_{TH} Z_{MG} cos(\beta - \alpha)} \tag{5}$$

where α and β are the angles of Z_{MG} and Z_{TH} respectively.

Maximum apparent power of MG, represented as S_{MMG}, can be obtained as,

$$S_{MMG} = \frac{E_{TH}^2}{2V_{MG}I_{MG}[1 + \cos(\beta - \alpha)]} \tag{6}$$

S_{MMG} gives maximum loadability limit which depends on Thevenin parameters which vary with operating scenarios.

Islanding detection monitoring factor (IDMF) is formulated as difference between the microgrid's apparent power and its maximum apparent power and is given as,

$$IDMF = S_{MG} - S_{MMG} \tag{7}$$

$$\begin{aligned} IDMF = E_{TH}^2 \big(&\big(V_{MG}I_{MG}(1 + 2V_{MG}I_{MG}) - Z_{TH}^2\big) \\ &+ 2V_{MG}I_{MG}cos(\beta - \alpha)(Z_{TH} + (V_{MG}I_{MG}))\big) \end{aligned} \tag{8}$$

Thus with two bus Thevenin equivalent circuit any system parameter variations in UG and microgrid can be observed at PCC. Normally, IDMF has a high magnitude and it is network dependent. IDMF with negative sign indicates an islanding event. With increase in load, Thevenin impedance increases and under islanding conditions, IDMF shows sudden change in the value. IDMF acts a gauge for maximum loading capability for any event in the UG or MG. However, simulation studies showed that IDMF is incapable to distinguish between islanding and other transient events in case of power export especially when the power mismatches are low. Analyzing this behavior of IDMF, to make the IDA free of nuisance trippings, a new index is proposed and considered along with it.

B. *Rate of Change of Inverse Hyperbolic Cosecant Function*

Inverse hyperbolic functions involve natural logarithmic function. Even minute variations in voltage can be maximized using inverse hyperbolic function which would make IDA prompt. Compared to inverse hyperbolic secant function [17] inverse hyperbolic cosecant function (IHCF) [18] gives a more magnified variation in voltage.

IHCF of voltage is expressed as,

$$IHCF = \ln\left(\frac{1 + \sqrt{1 + V^2}}{V}\right) \tag{9}$$

where, V is rms voltage $\forall\ V \neq 0$.

Superiority of IHCF is its proportional additive changes in the variable as in (9), compared to inverse hyperbolic secant function expressed in (10).

$$IHSF = \ln\left(\frac{1 + \sqrt{1 - V^2}}{V}\right) \tag{10}$$

By taking Δt as the sampling interval, rate of change of IHCF (ROCIHCF) is given by,

$$ROCIHCF = IHCF/\Delta t \tag{11}$$

C. *Islanding detection indicator*

Though combined use of IDMF and ROCIHCF, results in reduced NDZ and can discriminate IEs from non-islanding events, it resulted in false alarms during short circuit faults involving ground in nearby feeders. Thus, voltage is also considered along with the indices. Proposed IDA may be logically summed up as an indicator named, islanding detection indicator and is defined in (12) as,

Islanding detection indicator (IDI) =

$$\begin{aligned} &\big((IDMF < \mu)OR\big(\kappa_{Lo} \leq ROCIHCF \leq \kappa_{Up}\big)\big) \\ &AND \\ &\big((v_{minUp} \geq V \geq v_{minLo})OR(V \geq v_{Ul})\big) \end{aligned} \tag{12}$$

where μ is IDMF threshold, κ_{Lo}, κ_{Up} are lower and upper limits of ROCIHCF. v_{minUp}, v_{minLo} are the ranges for minimum values of voltage and v_{Ul} represents the maximum value of voltage for the precise distinction between IEs and non-islanding event (NIEs). IDI is either 1or 0: where one indicates an IE whereas zero indicates NIE.

Threshold values are decided through exhaustive simulations for several events and operating scenarios to prevent spurious alarms. To detect an IE, threshold values of the indices are obtained as IDMF < (−400) and 0.1 ≤ ROCIHCF ≤ 1.1. Voltage reduced drastically for three phase and line faults involving ground which were cleared after 0.1 s on initiation of the fault. However, it is a transient condition and should not be misinterpreted as an IE. Therefore, minimum value of voltage should lie in the range of 0.86 p.u to 0.8 p.u. This constraint eliminates false alarms and meets the standards of voltage constraint of 0.85 p. u and 1.1p.u. In the system studied, during power export, it was noticed that voltage at the PCC bus maintained a voltage near to 1.0 p.u during islanding conditions. Therefore, here, in order to recognize IEs during zero, and other different power mismatch ratios, upper threshold of voltage is fixed at 1.0 p.u. All the indices are computed in every half cycle.

3.2 *Case 2: Loss of Feeder Connected to DG in MG*

Any feeder loss connected to a DG causes its separation from the utility and therefore needs to be monitored. If DG's output power matches with the load powers in the sub-island, DG need not be disconnected and can have an islanded operation within the system voltage and frequency constraints. However, in this situation

resulting in minute changes in voltage and frequency cannot be detected by voltage and frequency relays. In this scenario, current relays at the DG terminals can be utilised to communicate to the control center. Then, at the MGCC, PoB in that sub-microgrid is compared to the threshold as would be explained in Sect. 6. For islanded management of the sub-microgrid the transition time to isolated management mode should be in the time span for which the power balance is sustained in the islanded network. Else, the DG should be tripped.

3.3 Case 3: Persistent Fault in MG

A persistent fault in any feeder in MG may result in CB operation leading to DG tripping. Therefore, such faults should be detected faster. For early detection of persistent faults within the MG, concept of mathematical morphological filters (MMF) is adopted for time series analysis of fault current. Dilation and erosion operators for fault current with structural element (SE) of length and height of 3 and 0.01 respectively are given by (13) and (14).

Dilation operator for fault current, $I_f(k)$ [19] is given as,

$$\left(I_f \oplus SE_n\right)(k) = max\left\{I_f(k - s) + SE(s)\right\} \tag{13}$$

Erosion operator for $I_f(k)$ is given by (14) as,

$$\left(I_f \ominus SE_n\right)(k) = min\left\{I_f(k + s) - SE(s)\right\} \tag{14}$$

where $I_f(k)$ and $SE(k)$ represent the function of the fault current and structural element with $SE_n = [0.01, 0.01, 0.01]$; k and s are integers with $k = (1, 2 \ldots N)$, N being number of samples in the input signal, $s = (1, 2 \ldots m)$ denoted the elements in the SE and $m < N$, m being length of SE.

Average of the dilation and erosion operators gives the dilation and erosion median filter (DEMF) and is given as,

$$DEMF_n(k) = \frac{1}{2} * \left(I_f \oplus SE_n + I_f \ominus SE_n\right) \tag{15}$$

where $n = (1, 2, \ldots, m)$.

Then ΔI_f is the difference of $DEMF_n$ from $I_f(k)$ and is expressed as,

$$\Delta I_f(k) = I_f(k) - \left(\frac{DEMF_1(k) + DEMF_2(k) + \cdots + DEMF_m(k)}{m}\right) \tag{16}$$

Thus fault detector is defined as the absolute value of the difference between ΔI_f at every consecutive intervals given by (17),

$$\Delta DEMF_n(k) = \left| \Delta I_f(k+1) - \Delta I_f(k) \right| \qquad (17)$$

From the simulation studies it has been concluded that a persistent short circuit fault is identified when ΔDEMF exceeds 111% of its nominal value for more than 6 cycles. Then the DG can be initiated for an islanded operation satisfying the PoB constraints. Depending on PoB, DG may be disconnected or isolated. This also avoids spurious disconnection for transient short circuit faults. Flow diagram of the proposed IDA is shown in Fig. 4. System parameters read from PMUs installed in two buses are used to calculate the indices. If IDI is 1, an IE is detected to manage the whole microgrid for an islanded operation. At the same time, IDA checks for any loss of feeder in the MG and feeder current is monitored. A trend of current magnitude prone to zero is communicated to MGCC by current relay. Any persistent short circuit fault is recognized rapidly by the fault detector operator given by (12) and communicated to the MGCC. For case 2 and case 3, islanded operation is decided based on PoB in the sub-microgrids.
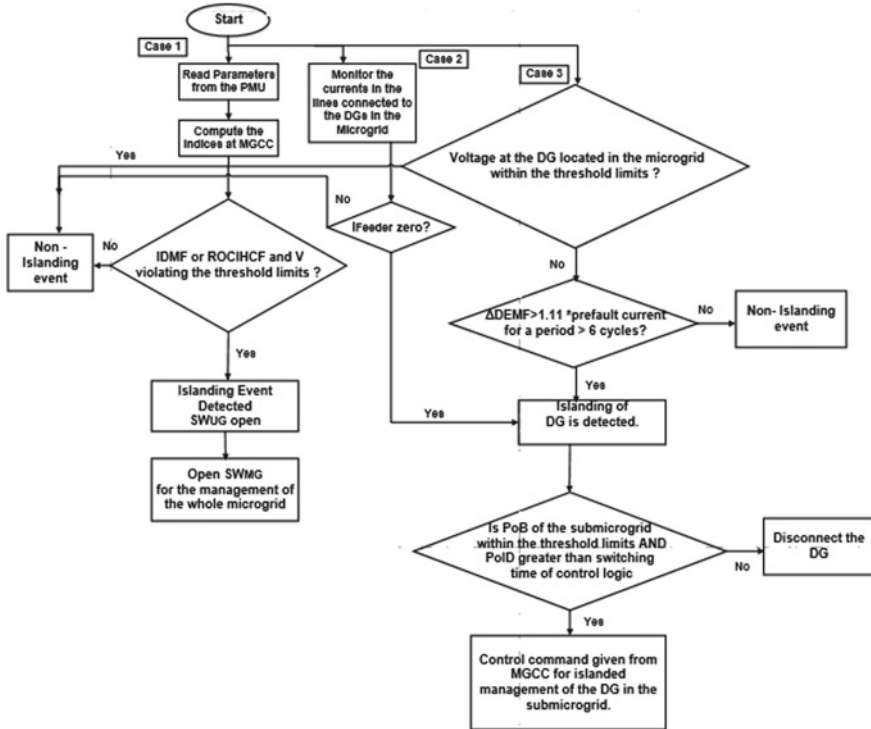

Fig. 4 Functional flowchart depiction of the proposed IDA

4 Result Analysis

System [7] shown in Fig. 5 is a balanced network of 120 kV with 2 step down transformers of rating 120 kV/25 kV. Three distribution feeders spread from 25 kV bus, which acts as the utility PCC. The DG system consists of two 9 MW wind farms at 575 V, 60 Hz with six wind turbines of 1.5 MW and 1 synchronous diesel engine with Woodward governor model of 2.5 MW,3.125 MVA,575 V,60 Hz. Loads are modelled as constant impedance models. Rated short circuit MVA is 2500 MVA. The whole microgrid can be considered as a superset of networked sub-microgrids. Three sub-microgrids are microgrid 1, microgrid 2 and microgrid 3 as represented in Fig. 5. The sampling rate is 3.6 kHz at 60 Hz nominal frequency. The simulation period is 1 s. Modelling of test system and simulations are conducted in PowerFactory and IDA in MATLAB 2012b in an Intel Core i5 3470, 8 GB RAM, 3.2 GHz processor.
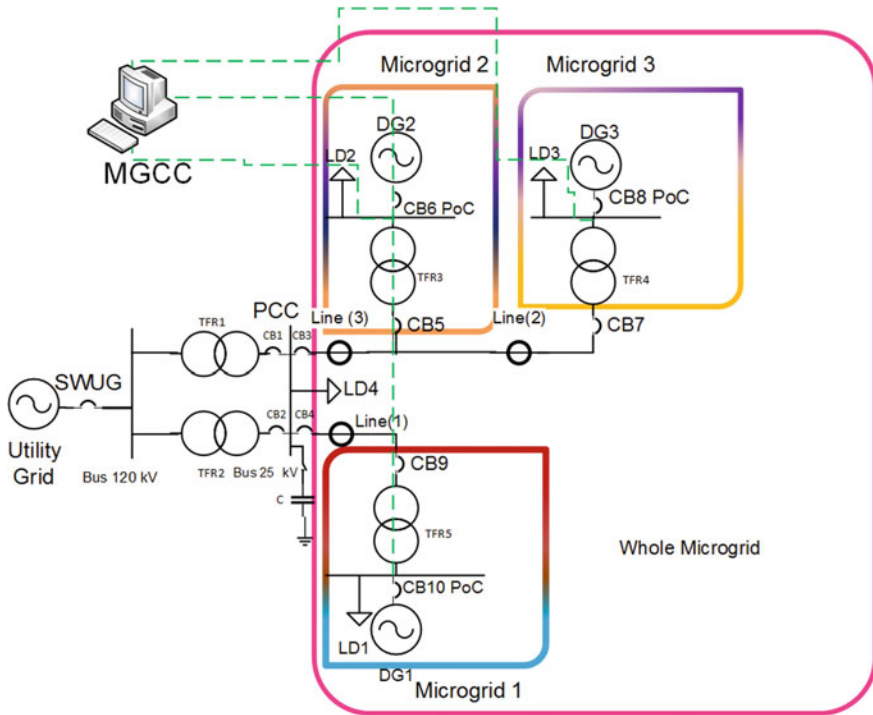

Fig. 5 Test system under study

4.1 Case 1

For IE such as opening of CB1 and CB2 or SW$_{UG}$, a trip command is given to island the whole MG at t = 0.5 s. Simulation studies have been carried out while importing active power by keeping DG generation levels fixed and varying the feeder load. Zero active power mismatch is observed at 40% feeder load. 5, 10 and 20% of power mismatches are observed when load is 50%, 60% and 70% of its nominal value. The IDA is able to identify the islanding conditions for the selected threshold values of ROCIHCF. Magnitude of ROCIHCH increases on islanding. IDMF also reduces below its threshold for all the power mismatches. Figure 6 shows change in voltage at the PCC for various for the above IEs. It can be observed that for these events voltage infringes the threshold. It may be noted that, voltage too falls between 0.86 and 0.8 along with IDMF and ROCIHCF indicating an IE. All the above IEs performed are tabulated in Table 1.

If IDMF or ROCIHF violates its threshold constraints and if voltage too breaches its constraints, trip command is signalled to the whole MG as IDI is 1 for all the power scenarios. From Table 1, it is concluded that islanding detection time is 5 ms irrespective of power mismatch ratios. The negative power magnitudes in the table
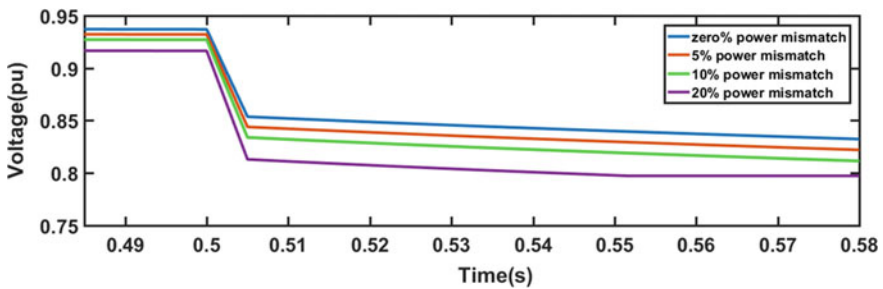

Fig. 6 Voltages at PCC for various active power mismatches

Table 1 Parameters for islanding condition at different power mismatches

Active power mismatch (%)	Detection Time (ms)	IDMF	ROCIHCF	V(p.u)	IDI
−20	5	−464157	0.15	1	1
−10	5	−53793	0.07	1	1
−5	5	−6975	0.03	1	1
0	5	−2428	0.30	0.85	1
5	5	−2086	0.32	0.84	1
10	5	−1652	0.33	0.83	1
20	5	−985	0.36	0.81	1

Table 2 IDI for cases 2 and 3 in the microgrid

Line connected	IDI for case 2	IDI for case 3	IDI for case 3
Line1	1	0	0
Line2	0	1	1
Line3	0	0	1

indicate export of power. The chosen threshold ensures minimum islanding detection time. Likewise, simulation studies have been done for reactive power export scenarios.

4.2 Case 2

Loss of Line 1, Line 2 or Line 3 leading to open conditions of CB6, CB8 or CB10 respectively are considered here. Column 2 of Table 2 indicates islanding detection index at PoC for loss of Line 1. For these faults, IDI at the PCC would be zero. On detecting Line 1 current to be zero, protective relay at the DG terminal signals to MGCC for islanded management. For loss of Line1 connected to microgrid 1, IDI is high only for Line1. Current and voltage are within their threshold limits for other lines as per the algorithm. Thus sub-microgrids 2 and 3 remain intact and PoB of sub-microgrid 1 decides its further operation.

4.3 Case 3

This case is evaluated for two scenarios and tabulated as columns 3 and 4 in Table 2. It is observed in column 3 that IDI is 1 for Line 2 outage. For the other two lines IDI is zero. Last column indicates IDI for simultaneous outage of Line 2 and Line 3.

Figure 7 shows current in Line1 normalized with respect to its peak value. A 3 phase fault in Line1 at 0.5 s is shown in Fig. 8a. MMF is applied to the normalized current as explained before. Then, DEMF and ΔDEMF are computed. It may be seen that ΔDEMF is exceeding 0.1 pu which is 111% greater than its nominal value for more than 0.1 s. However, for a fault which is cleared in 0.1 s depicted in Fig. 8b, shows that ΔDEMF exceeds the threshold at the fault initiation but thereafter lowers to 0.099 p. u. when fault is cleared. Thus IE can be detected even before circuit breaker opens. Further examination of ΔDEMF output showed that it remained under the threshold for other oscillatory events in the MG. Thus the MMF needs to be functioning for each DGs existing in the grid.
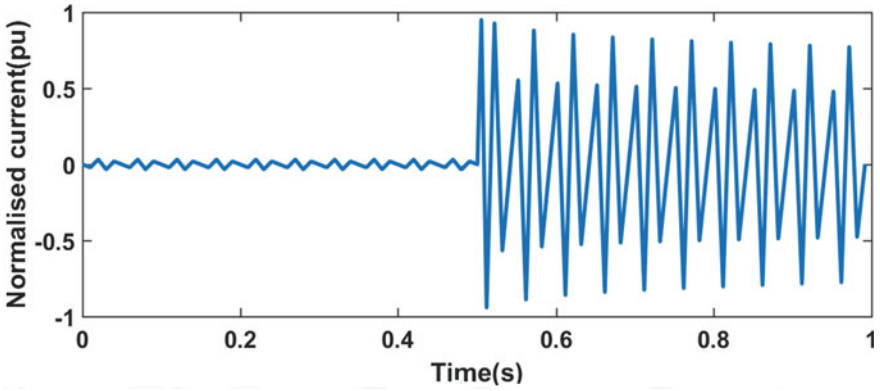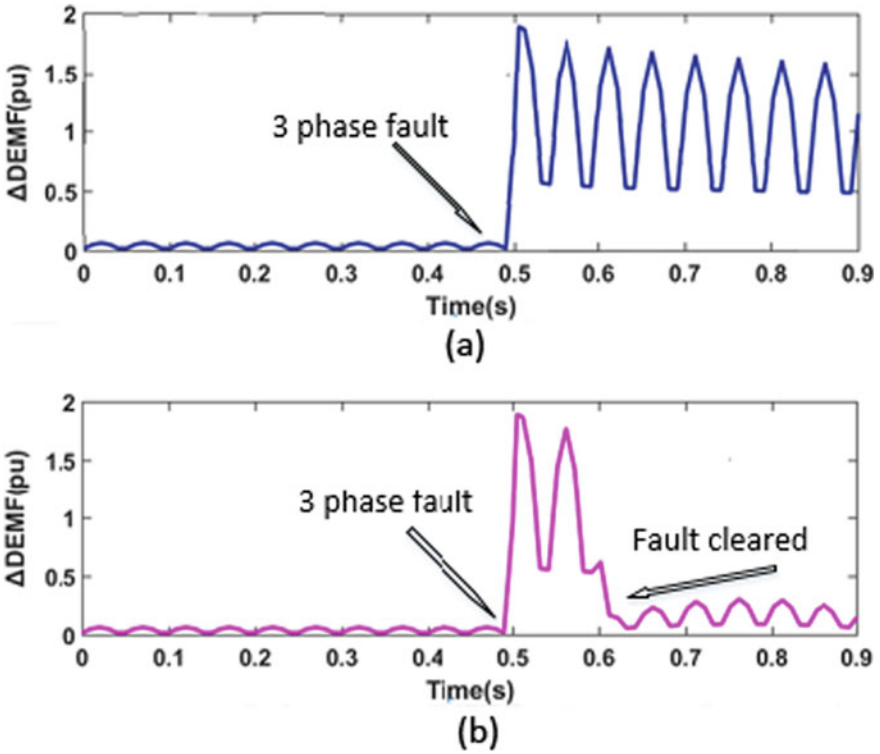
Fig. 7 Normalized current in Line1

Fig. 8 Current in Line1 **a** 3 phase persistent fault; **b** 3 phase temporary fault

4.4 Performance Evaluation *of* the IDA for Transient Events

Transient events such as transformer and capacitor switching, network topology change, parallel feeder loss, and connection/disconnection of single and multiple DGs have been simulated to evaluate robustness of the IDA for non-islanding events. Figure 9a depicts variation in voltage for different DG disconnections. The figure confirms that voltage satisfies the threshold range for each case. Capacitor bank switching to adjust the power factor can give rise to voltage swing. This phenomenon may be misinterpreted as an IE. To check stability of the IDA, a capacitor of 8.5 μF connected at the PCC is stepped up to 850 μF in steps of three. Figure 9b proved IDA's prowess to distinguish IE from transient events.

Islanding detection techniques usually misconstrue three-phase fault involving ground in nearby feeders as IEs [7]. Robustness of the IDA in eliminating false alarms for faults which are cleared at different locations along the feeder length, each with different values of fault resistance have been evaluated. The algorithm did not create false alarms during these scenarios. Figure 10 shows that, for single line to ground (LG faults in line (2) and line (3)) and three phase faults, voltage reduces extremely. However, an event shall be classified as islanding only if magnitude of voltage is between 0.86 and 0.8 p.u.
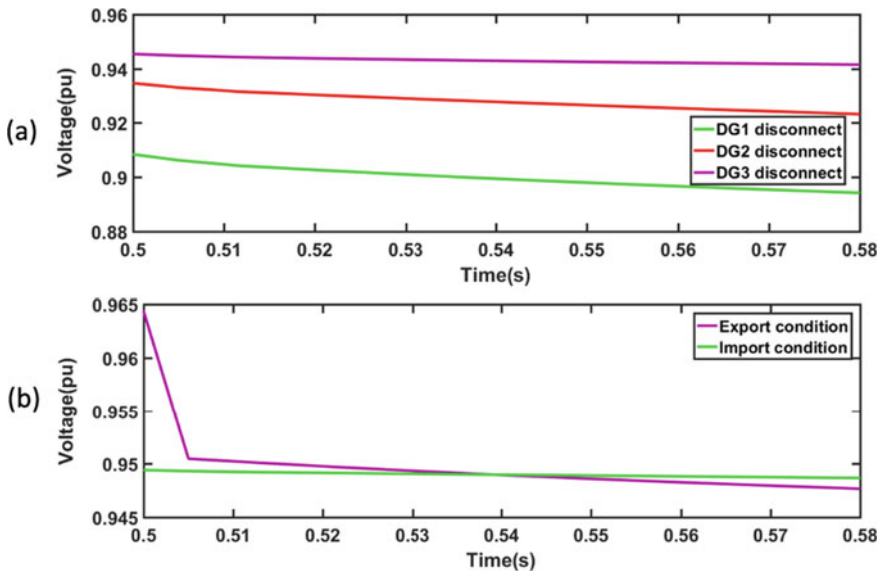

Fig. 9 PCC voltage in MG **a** DG disconnection; **b** Capacitor bank switching during export/import conditions
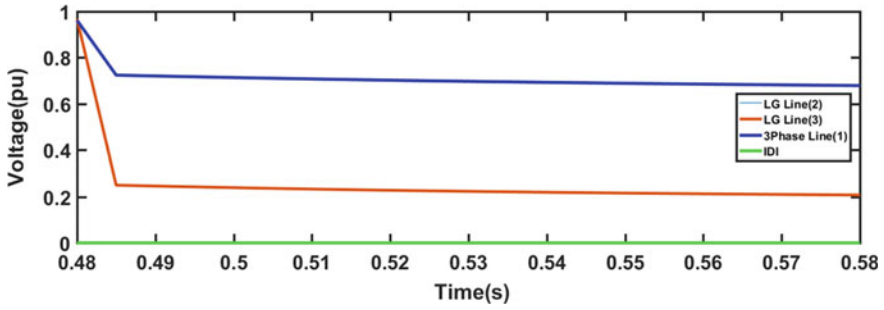
Fig. 10 PCC voltage for various faults

For analysing the performance during change in network configuration, tie-switch SW1 which is normally open, is closed as shown by red ellipse in Fig. 11. IDI remains zero and hence the algorithm precisely identified it as a non-islanding event.
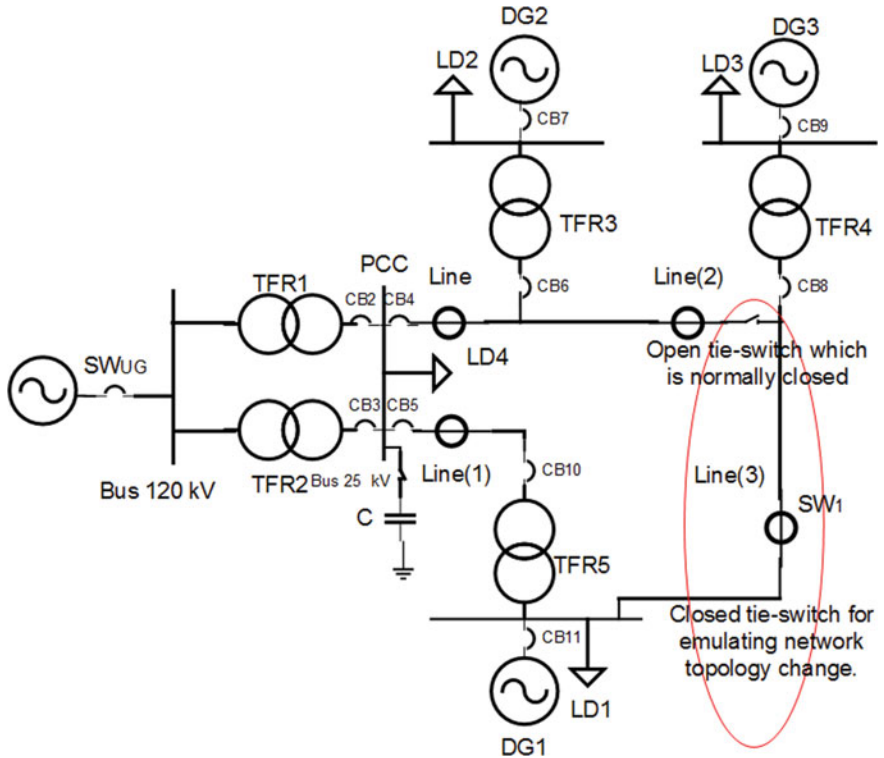

Fig. 11 Microgrid depicting network topology change in DIgSILENT/PowerFactory

5 Economic Analysis of the Proposed IDA with Minimal Placement of PMUs

As per [20] reducing number of buses where PMUs are deployed does not lead to significant decrease in its deployment cost. However, the authors have performed an economic analysis with deployment of two PMUs with respect to number of sub-microgrids going to islanded operation instead of being disconnected and analysed the reduction in cost of consumer outage with their islanded operation. Thus here minimal PMU placement refers to the two PMUs deployed at the PCC of the whole MG with the UG and the reference bus in the UG. When load and generation in the microgrid matches, at the instant of disconnection from utility, an islanded operation of the DG is possible [21]. Hence it becomes necessary for a probabilistic analysis considering the intermittent and uncertain nature of NDRES in microgrid. To avoid redundant DG disconnection in the sub-microgrids, probability of power balance (PoB) is introduced [22].

5.1 Probability of Power Balance and Microgrid Performance Index

PoB is defined as the probability density function of the ratio of total power demand to the total power generation in the islanded sub-microgrid. PoB in sub-microgrids 1, 2 and 3 can be expressed by (18)–(20). Sub-microgrid 1 consists of 9 MW wind plant and load of 8 MW, sub-microgrid 2 represents 9 MW wind plant with 2.5 MW load. A 2.5 MW diesel generator feeding 8 MW load constitute sub-microgrid 3. The sources and loads are assumed to maintain a power factor of 1.

$$PoB_1 = PDF1 \left[\frac{\sum_{i=1}^{N} PL_{SMG1} + jQL_{SMG1}}{P_{SMG1} + jQ_{SMG1}} \right] \tag{18}$$

$$PoB_2 = PDF2 \left[\frac{\sum_{i=1}^{N} PL_{SMG2} + jQL_{SMG2}}{P_{SMG2} + jQ_{SMG2}} \right] \tag{19}$$

$$PoB_3 = PDF3 \left[\frac{\sum_{i=1}^{N} PL_{SMG3} + jQL_{SMG3}}{P_{SMG3} + jQ_{SMG3}} \right] \tag{20}$$

where PDF1, PDF2 and PDF3 are probability density functions with a normal distribution as given in (21) for sub-microgrids 1, 2 and 3 respectively.

$$PDF = \frac{1}{\sigma \sqrt{2\pi}} * e^{\frac{-(A-\mu)^2}{2\sigma^2}} \tag{21}$$

where A defines ratio of output power of DG to the load, μ and σ denote mean and standard deviation respectively.

PL_{SMG}, QL_{SMG} denote real and reactive power demands in the microgrid and P_{SMG}, Q_{SMG} are the real and reactive power generation from the sources in the microgrid.

Islanded operation is possible when PoB lies between 0.95 and 1.5 to accommodate any NDZ [22]. Lower threshold of 0.95 is adopted to include the situation where generation exceeds load. The upper value accommodates system losses in the sub-microgrids. PoB threshold is then chosen as,

$$0.95 < \text{PoB} < 1.5 \tag{22}$$

Time span during which the island satisfies the PoB limits can be defined as duration of probability of operation (PoID) in islanded mode,

$$PoID = n * t \tag{23}$$

where n represents instants of time when PoB satisfies the constraints, t being sampling rate. Time required to change from grid tied to islanded mode for converters has been approximated to be as under 640 ms as per [14].

Sampling rate is 10 ms with delay in communication assumed as 20 ms [14]. PoB obtained for sub-microgrids 1 and 2 are illustrated in Fig. 12a. Relay senses and communicates to the MGCC when CB5 connecting to sub-microgrid 2 is opened. As PoB is not satisfying the threshold, instantaneous measure would be to detach the wind plant. To evaluate the proposed IDA for IEs in the microgrid an index is formulated. Microgrid Performance Index (MGPI) is the ratio of number of autonomous sub-microgrids on islanding detection to number of IEs identified at the PoC.

$$MGPI = \frac{\sum_{i=1}^{n} N\_SMG_i}{\sum_{j=1}^{m} W_j} \tag{24}$$

where N_SMG is number of autonomous sub-microgrids determined based on PoB, n is total number of sub-microgrids, Wj represents total number of breaker openings and m denotes number of PoCs.

Thus MGPI yields the following conditions,

$$MGPI = \begin{cases} > 1; & for\ successful\ submicrogrid\ management \\ 0; & otherwise \end{cases} \tag{25}$$

PoB for sub-microgrid 1 is 0.96 when CB9 is opened at 0.52 s. It falls inside PoB limits. PoID has been found to be 60 ms as shown in Fig. 12b. Likewise, for circuit breaker openings of CB5, CB7 and CB9, two sub-microgrids could be managed in islanded mode out of the three sub-microgrids in the test system considering the PoB.

(a)

(b)
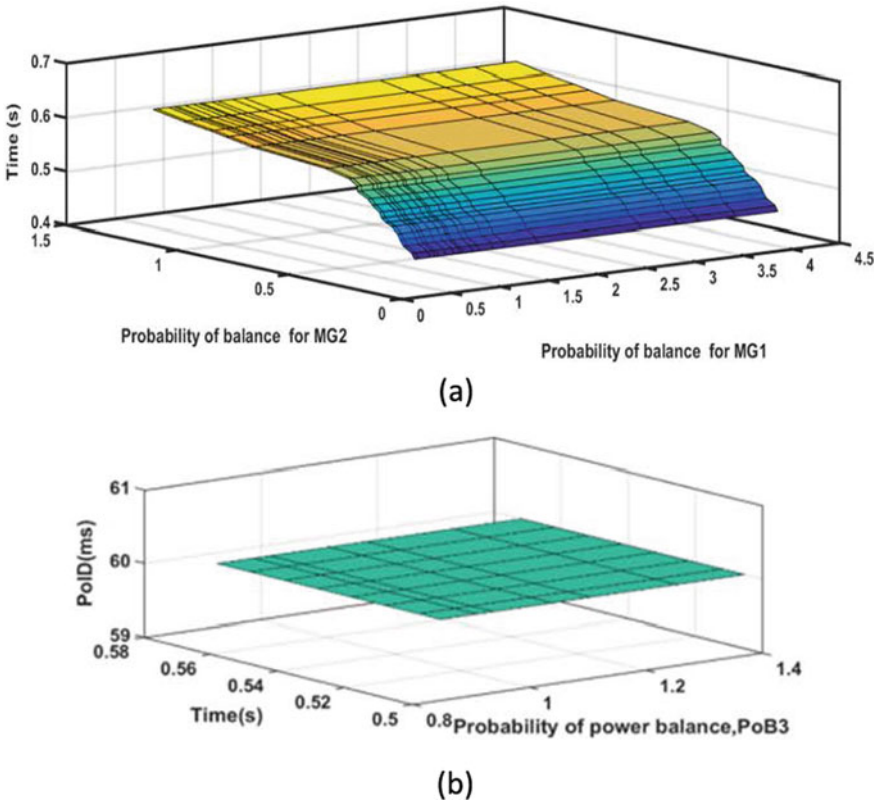
Fig. 12 **a** PoB of sub-microgrid 1, sub-microgrid 2; **b** PoID with respect to islanding time and PoB of MG1

DG in sub-microgrid 2 only had to be disconnected. This results in an MGPI value of two, stipulating proper microgrid utilization instead of disconnecting all the DGs.

5.2 Reliability Benefit for Microgrid Under Islanded Operation

A lower MGPI indicates increased average energy not supplied (AENS) by the sub-microgrid. Thus, to assess economic benefit for microgrid with the proposed IDA, reliability benefit is defined as the reduction in cost of consumer power outage. It also involves reduction in installation cost of PMU at each bus. Thus reliability benefit with islanded sub-microgrids (RB_{ISMG}) is expressed as,

$$RB_{ISMG} = COC_r + CPMU_r \tag{26}$$

where COC_r is reduced customer outage cost and $CPMU_r$ is reduced PMU installation cost expressed as in (27) and (29)

$$COC_r = (COC - COC_{ISMG} * t_d \tag{27}$$

COC and COC_{ISMG} refer to customer outage cost when all the sub-islands are disconnected and customer outage cost for sub-microgrid disconnected based on MGPI.

Where

$$COC = \sum_{j=1}^{l} RIE_j * ENS_j \, \$/t_d \tag{28}$$

$$L = l - N\_SMG$$

RIE is rate of interrupted energy \$/KWh, ENS is energy not supplied KWh/t_d, t_d is duration of islanded operation assumed as 1 h for the study.

Reduced PMU installation cost is defined as,

$$CPMU_r = CPMU - CPMU_{ISMG} \tag{29}$$

$CPMU$ and $CPMU_{ISMG}$ refer to PMU installation cost at all the buses and PMU installation cost in two buses as envisaged in the proposed IDA respectively.

where

$$CPMU = \sum_{i}^{b} C_{iPMU} * x_i \tag{30}$$

C_{iPMU} is PMU installation cost at bus i, $x_i = 1$; if PMU deployed in bus i.

RIE for load is assumed as 1000 \$/KWh and PMU installation cost is 40,000 \$ [23].

For the case considered, an economic analysis has been carried out using the proposed reliability benefit index. In Table 3, COC_r gives the economic benefit when all three sub-microgrids are disconnected versus two and one possible sub-microgrids that can be autonomously managed during the islanded duration. $CPMU_r$ indicates the difference in installation cost when PMUs are installed at all the buses and PMUs installed at two buses as proposed in this work. Thus it may be concluded that, as

Table 3 Reliability benefit index for microgrid

MGPI	COC_r (10^4\$)	$CPMU_r$ (10^4\$)	RB_{ISMG}(10^4\$)
2	10,240	16	1040
1	512	16	528

the number of islanded sub-microgrids increases or as MGPI increases, reduction in customer outage costs increase profoundly. Moreover, minimal placement of PMUs minimizes total cost associated with minimize a total cost associated with PMU failures and cost of its restoration and cost of communication links between PMUs.

## 6 Decision Tree Technique for Islanding Detection in Real Time

For quick islanding detection in real time, decision tree (DT) technique has been adopted. Initially, this study has used 50% of the data as training and remaining 50% as test set using percent split validation method. The two indices and voltage at the utility PCC are used as attributes with islanding detection index (IDI) as target obtained from offline testing and given as input to SPSS®IBM statistics for building DT model. Predictive scoring for real time analysis is performed using the DT model built. For IE at zero power balance situation, out of 5043 instants, 4038 non islanding cases are identified as NIE and one non islanding case has been misclassified as IE. However, all the 1004 islanding cases are classified as IEs as shown in Table 4. To compare the model predictions with the actual data, a correlation table is built as in Table 5. From the table, it may be observed that, a correlation of 0.984 between the model IDI and the predicted IDI for the real data using Pearson coefficient indicates a very high positive correlation between the actual and predicted islanding index. This also substantiates the selection of the threshold value. Thus the model is successful with a reliability of 100% with an accuracy of 99.97%.

Table 4 Classification table

Predicted				
Data	Observed	Non islanding	Islanding	%correct
	Non islanding	4038	1	99.97
	Islanding	0	1004	100
	Overall Percentage	80.1%	19.9%	100

Table 5 Correlation table of a real event with simulated DT model

Correlation		IDI	Predicted IDI
IDI	Pearson	1	0.984
Predicted IDI	Pearson	0.984	1
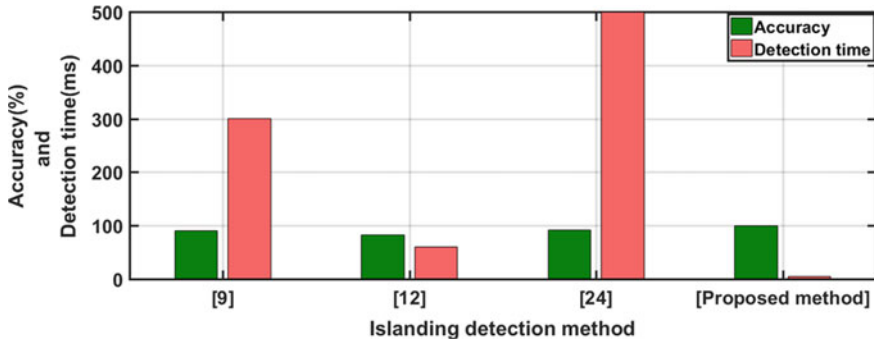
Fig. 13 Comparison of accuracy and detection times of the proposed method with contemporary works

7 Comparison of the Proposed IDA with Recent Works

The proposed IDA$_{UPCC}$ has been compared with recently published schemes and presented in Fig. 13. Among these [9] have IDTs deployed at the PCC as well as the PoC of each DG terminal while Ref. [12] has the IDT deployed in the PCC. Islanding detection algorithm in [24] works at each DG terminal using an ANN classifier based on transient response data from synchrophasor units. It is observed from the figure that the proposed IDA has better features with faster response and higher accuracy compared to others. Reference [24] has the lowest response time with 0.5 s while IDA$_{UPCC}$ detects islanding event in 5 ms.

As a future work and research gaps, the applications of PMU and wide-area monitoring systems in modern power systems operation, control, stability, protection and security should be well-investigated [25–30]. PMUs are the backbone of wide are monitoring system that can improve the overall security and stability of power systems. Therefore, it is suggested to make in-depth evaluation of the power system security under the new environment control based one PMUs data. Likewise, new WAMS-based methods are in demand for improving the islanding detection in future smart grids [31–33].

8 Conclusion

A reliable and accurate islanding detection algorithm is proposed here with minimal PMU deployment and maximum reduction in customer outage cost. The IDA works from the utility PCC with sturdy communication infrastructure, instead of being implemented at the DG terminals. Islanding detection monitoring factor, rate of change of inverse hyperbolic cosecant function of voltage are utilized along with the magnitude of voltage at utility PCC to make the whole microgrid manage an islanded operation. Distinctive features of the IDA are its zero non-detection zone,

islanding detection time of 5 ms irrespective of percentage of power mismatches and ability to reduce false alarms. Thus the IDA with two PMUs deployed in the system prevents redundant DG disconnection for fault events in the sub-microgrids. For persistent fault in the sub-microgrid, probability of power balance in the sub-microgrids determines whether the DG has to be disconnected or considered for islanded operation. Economic analysis for reduction in customer outage costs has been performed which indicates greater reliability benefits with higher microgrid performance index. Real time DT testing proved robustness of the proposed IDT with hundred percent accuracy.

References

1. B. Matic-Cuka, M. Kezunovic, Islanding detection for inverter- based distributed generation using support vector machine method. IEEE Trans. Smart Grid. **5**(6), 2676–2686 (2014)
2. IEEE standard for interconnecting distributed resources with electric power systems – amendment 1, IEEE Std 1547a-2014 (Amendment to IEEE Std 1547–2003) (2014)
3. C. Seung-Tae, Real-time analysis of an active distribution network - coordinated frequency control for islanding operation, Dissertation for the Doctoral Degree, Technical University of Denmark (2012)
4. G. Buigues, A. Dysko, V. Valverde, I. Zamora, E. Fernandez, Microgrid protection: technical challenges and existing techniques, in *Proceedings of International Conference Renewable Energies Power Quality*, Bilbao, Spain, Mar 2013, pp. 222–227
5. S. Chowdhury, S.P. Chowdhury, P. Crossley, *Microgrids and Active Distribution Networks* (IET Renewable Energy Series 6) (Institute of Engineering Technology, London, U.K., 2009)
6. K. Sareen, B.R. Bhalja, R.P. Maheshwari, Universal islanding detection technique based on rate of change of sequence components of currents for distributed generations. IET Renew. Power Gener. **10** (2), 228–237 (2016)
7. M.A.Farhan, K.S Swarup, Mathematical morphology-based islanding detection for distributed generation. IET Gener. Transm. Distrib. **10**(2), 518–525 (2016)
8. R. Nale, M. Biswal, N. Kishor, A Transient component based approach for islanding detection in distributed generation. IEEE Trans. Sustain. Energy (2018). https://ieeexplore.ieee.org/document/8424028
9. A.G. Abd-Elkader, S.M. Saleh, M.B. Magdi Eiteba, A passive islanding detection strategy for multi-distributed generations. Electr. Power Energy Syst. **99**, 146–155 (2018)
10. O. Palizban, K. Kauhaniemi, J.M. Guerrero, Microgrids in active network management- Part II. Renew. Sustain. Energy Rev. **36**, 440–451 (2014)
11. IEEE standard for Interconnection and Interoperability of Distributed Energy resources with Associated Electric Power Systems Interfaces, IEEE Std. 1547 (2018)
12. C.N. Papadimitriou,V.A. Kleftakis, N.D. Hatziargyriou, A novel islanding detection method for microgrids based on variable impedance insertion. Electr. Power Syst. Res. **121**, 58–66 (2014)
13. M. Vatani, M.J. Sanjari, G.B. Gharehpetian, Islanding detection in multiple-DG microgrid by utility side current measurement. Int. Trans. Electr. Energy Syst. **25**(9), 1905–1922 (2015)
14. D. Shi, R. Sharma, Y. Ye, Adaptive control of distributed generation for microgrid islanding, in *4th IEEE PES Innovative Smart Grid Technologies Europe (ISGT Europe)* (Copenhagen, 2013), pp. 1–5
15. M.A. Hossain, H. Pota, M.J. Hossain, A.M.O. Haruni, Active power management in a low-voltage islanded microgrid. Int. J. Electr. Power Energy Syst. **98**, 36–48 (2018)
16. K. Vu, M. Begovic, D. Novosel, Use of local measurements to estimate voltage stability margin. IEEE Trans. Power Syst. **14**(3), 1029–1035 (1999)

17. K. Sareen, B.R. Bhalja, R.P. Maheshwari, Islanding detection technique based on inverse hyperbolic secant function. IET Renew. Power Gener. **10**(7), 1002–1009 (2016)

18. M. Trott, Inverse trigonometric and hyperbolic functions. In Mathematica Guide book for programming, 2004 ed. (New York, Springer-Verlag, 2004)

19. S. Gautam, S.M. Brahma, Detection of high impedance fault in power distribution systems using mathematical morphology. IEEE Trans. Power Syst. **28**(2), 1226–1233 (2013)

20. A. Pal, A.K.S. Vullikanti, S.S. Ravi, A PMU placement scheme considering realistic costs and modern trends in relaying. IEEE Trans. Power Syst. **32**(1), 552–561 (2017)

21. R. Bründlinger, B. Bletterie, Unintentional islanding in distribution grids with a high penetration of inverter-based DG: Probability for islanding and protection methods, in *Proceedings of IEEE Russia Power Technology Conference*, St. Petersburg, Russia, 2005, pp. 1–7

22. R. Rohikaa Micky, A. Sankar, R. Sunitha, A combined islanding detection algorithm for grid connected multiple microgrids for enhanced microgrid utilization. Int. Trans. Electr. Energy Syst. e12232 (2019). https://doi.org/10.1002/2050-7038.12232

23. U.S. Department of Energy, Office of Electricity Delivery and Energy Reliability, Factors affecting PMU installation costs (Oct 2014). https://www.smartgrid.gov/files/PMU-cost-study-final10162014_1.pdf

24. D. Kumar, P. Sarathee Bhowmik, Artificial neural network and phasor data based islanding detection in smart grid. IET Gener. Transm. Distrib. **12**(21), 5843–5850 (2018)

25. H.H. Alhelou, M.E. Hamedani-Golshan, R. Zamani, E. Heydarian-Forushani, P. Siano, Challenges and opportunities of load frequency control in conventional, modern and future smart power systems: a comprehensive review. Energies **11**(10), 2497 (2018)

26. H.H. Alhelou, M.E. Golshan, J. Askari-Marnani, Robust sensor fault detection and isolation scheme for interconnected smart power systems in presence of RER and EVs using unknown input observer. Int. J. Electr. Power Energy Syst. **99**, 682–694 (1 Jul 2018)

27. H. Haes Alhelou, M.E. Hamedani Golshan, M. Hajiakbari Fini, Wind driven optimization algorithm application to load frequency control in interconnected power systems considering GRC and GDB nonlinearities. Electr. Power Compon. Syst. **46**(11–12), 1223–38 (21 Jul 2018)

28. H.H. Alhelou, M.E. Golshan, N.D. Hatziargyriou, Deterministic dynamic state estimation-based optimal lfc for interconnected power systems using unknown input observer. IEEE Trans. Smart Grid (9 Sep 2019)

29. H.H. Alhelou, M.E. Golshan, N.D. Hatziargyriou, A decentralized functional observer based optimal LFC considering unknown inputs, uncertainties, and cyber-attacks. IEEE Trans. Power Syst. **34**(6), 4408–4417 (2019). (May 13)

30. H.H. Alhelou, M.E. Golshan, T.C. Njenda, N.D. Hatziargyriou, An overview of UFLS in conventional, modern, and future smart power systems: challenges and opportunities. Electr. Power Syst. Res. **1**(179), 106054 (2020). (Feb)

31. R. Zamani, M.-E. Hamedani-Golshan, H. Haes Alhelou, P. Siano, H.R. Pota, Islanding detection of synchronous distributed generator based on the active and reactive power control loops. Energies **11**(10), 2819 (2018)

32. R. Zamani, M.E.H. Golshan, H.H. Alhelou, N. Hatziargyriou, A novel hybrid islanding detection method using dynamic characteristics of synchronous generator and signal processing technique. Electr. Power Syst. Res. **175**, 105911 (2019)

33. A. Abyaz, H. Panahi, R. Zamani, H. Haes Alhelou, P. Siano, M. Shafie-khahand, M. Parente. An effective passive islanding detection algorithm for distributed generations. Energies **12**(16), 3160 (2019)